Available online at www.sciencedirect.com
SCIENCE DIRECT®
Journal of Solid State Chemistry 179 (2006) 1965–1976
JOURNAL OF SOLID STATE CHEMISTRY
www.elsevier.com/locate/jssc

# Low-dimensional compounds containing cyano groups. XIV. Crystal structure, spectroscopic, thermal and magnetic properties of $[CuL_2][Pt(CN)_4]$ complexes ($L$ = ethylenediamine or *N*,*N*-dimethylethylenediamine)

Ivan Potočňák[a,*], Martin Vavra[a], Erik Čižmár[b], Katarína Tibenská[b], Alžbeta Orendáčová[b], Dirk Steinborn[c], Christoph Wagner[c], Michal Dušek[d], Karla Fejfarová[d], Harry Schmidt[c], Thomas Műller[c], Martin Orendáč[b], Alexander Feher[b]

[a]*Department of Inorganic Chemistry, Institute of Chemistry, P.J. Šafárik University, Moyzesova 11, SK-04154 Košice, Slovakia*
[b]*Centre of Low Temperature Physics of the Faculty of Science of P.J. Šafárik University and IEP SAS, Park Angelinum 9, SK-04154 Košice, Slovakia*
[c]*Institute of Inorganic Chemistry, Martin-Luther-University, Halle-Wittenberg, Kurt-Mothes-Street 2, D-06120 Halle, Germany*
[d]*Institute of Physics, Na Slovance 2, CZ-182 21 Praha 8, Czech Republic*

Received 28 February 2006; accepted 24 March 2006
Available online 1 April 2006

**Abstract**

Violet crystals of $[Cu(en)_2][Pt(CN)_4]$ and blue crystals of $[Cu(dmen)_2][Pt(CN)_4]$ were crystallized from the water–methanol solution containing $CuCl_2 \cdot 2H_2O$, ethylenediamine (en) or *N*,*N*-dimethylethylenediamine (dmen) and $K_2[Pt(CN)_4] \cdot 3H_2O$. Both compounds were characterized using elemental analysis, infrared and UV-VIS spectroscopy, magnetic measurements, specific heat measurements and thermal analysis. X-ray structure analysis revealed chain-like structure in both compounds. The covalent chains are built of Cu(II) ions linked by $[Pt(CN)_4]^{2-}$ anions in the [111] and [101] direction, respectively. The Cu(II) atoms are hexacoordinated by four nitrogen atoms in the equatorial plane from two molecules of bidentate ligands $L$ with average Cu–N distance of 2.022(2) and 2.049(4) Å, respectively. Axial positions are occupied by two nitrogen atoms from bridging $[Pt(CN)_4]^{2-}$ anions at longer Cu–N distance of 2.537(2) and 2.600(5) Å, respectively. Both materials are characterized by the presence of weak antiferromagnetic exchange coupling. Despite the one-dimensional (1D) character of the structure, the analysis of magnetic properties and specific heat at very low temperatures shows that $[Cu(en)_2][Pt(CN)_4]$ behaves as two-dimensional (2D) spatially anisotropic square lattice Heisenberg magnet, while more pronounced influence of interlayer coupling is observed in $[Cu(dmen)_2][Pt(CN)_4]$.


*Keywords:* 1D crystal structure; $[Pt(CN)_4]^{2-}$ anion; Hydrogen bonds; Thermal studies; Spectroscopic studies; Heisenberg square lattice

## 1. Introduction

Cyanide is an efficient ligand for the stabilization of the transition metals in either low or high oxidation states. This high electronic and coordinative versatility prompts its terminal coordination to almost all transition metals, and permits a wide number of binding modes in cyanide-bridged complexes. By far the most commonly observed binding modes are the terminal C-bond mode and the linear bridged arrangement. Differently bended bridged arrangements as well as various types of coordination to the three metals are much less common [1].

Because tetracyanoplatinate(II) anions can use a different number of cyano groups to bind to other metal atoms, they exist in a wide range of solid-state structures. When all

*Corresponding author. Fax: +421 55 62 221 24.
*E-mail address:* ivan.potocnak@upjs.sk (I. Potočňák).

0022-4596/$ - see front matter © 2006 Elsevier Inc. All rights reserved.
doi:10.1016/j.jssc.2006.03.033

four cyano groups are bound as monodentate ligands, it leads to the separation of ion pairs [2,3] (Scheme 1a). One structure has been reported very recently in which one of the four cyano groups acts as a bridging ligand and the resulting structure is a binuclear compound [4] (Scheme 1b). The bridging character of two cyano groups of $[Pt(CN)_4]^{2-}$ anion has been shown to yield several types of structures in the solid state. When two bridging cyano groups are in *cis*-arrangement three [5] (Scheme 1c) or four nuclear molecular compounds [6] (Scheme 1d) and zigzag chains [7] (Scheme 1e) are formed. When two bridging cyano groups are in *trans*-arrangement molecular [8] (Scheme 1f) or one-dimensional (1D) [9] (Scheme 1g) compounds are produced. According to our knowledge, only one compound exists containing two bridging cyano groups both in *cis*- and *trans*-arrangement resulting in three-dimensional (3D) structure [10] (Scheme 1h). Recently, the first example of three-dimensional structure in which three of the four cyano groups bridge two metal atoms was reported [11] (Scheme 1i). When all four cyano ligands are bridging, a molecular five nuclear complex cation [4] (Scheme 1j) or 3D structures [12,13] (Scheme 1k) can be isolated.

Recently, cyano complexes with various degrees of dimensionality have often been the subject of magnetic studies. In this case, the cyano group or cyano complex anion in addition to its structural function also exhibits an important electronic function: it forms an exchange path mediating the interaction among spins localized on paramagnetic centers. Dimensionality of a magnetic subsystem is fundamental for cooperation processes, but it does not mean that the magnetic and structural dimensionality must be the same. The increase of magnetic dimensionality can be caused by the influence of hydrogen bonds (HBs), $\pi$–$\pi$ and also dipole–dipole interactions [14,15].

Previous studies on the structure and magnetic properties of $[Cu(en)_2][Ni(CN)_4]$ [16,17] and also the isostructural $[Cu(en)_2][Pd(CN)_4]$ [18] revealed that despite the 1D character of their structure they behave as two-dimensional (2D) magnets. 2D character of the magnetic subsystem can be explained by the formation of HBs linking the neighboring chains and thus serving as exchange paths for magnetic interactions. The compounds with general formula $[Cu(L)_2][Ni(CN)_4]$, where $L = N$-methylethylenediamine or $N,N$-dimethylethylenediamine (dmen) were prepared [19] with the aim to suppress the formation of HBs. However, their study has shown that the formation of HBs was reduced only partially. Therefore, we have decided to change $[Ni(CN)_4]^{2-}$ anion by larger $[Pt(CN)_4]^{2-}$ anion with the expectation to suppress or at least to modify existing HBs. In this paper, we describe the preparation of $[Cu(en)_2][Pt(CN)_4]$ (**1**) and $[Cu(dmen)_2][Pt(CN)_4]$ (**2**) complexes along with their characterization using infrared (IR) and UV-VIS spectroscopy, thermal and X-ray crystal structure analyses, magnetic and specific heat measurements.

## 2. Experimental

### 2.1. Materials

Copper chloride dihydrate ($CuCl_2 \cdot 2H_2O$), en ($C_2H_8N_2$) and dmen ($C_4H_{12}N_2$) were of Merck quality and used as received. $K_2[Pt(CN)_4] \cdot 3H_2O$ was prepared according to the literature [20] using $H_2[PtCl_6] \cdot 6H_2O$ from Chempur as starting platinum containing material.

### 2.2. Synthesis

$[Cu(en)_2][Pt(CN)_4]$ (**1**). Into stirring water–methanol solution (1:1) of $CuCl_2$, ethylenediamine (en) (4 mmol) was added in one portion and after 30 min, aqueous solution of $K_2[Pt(CN)_4]$ (1 mmol) was added in one portion, too. In a few days, violet crystals of **1** were filtrated off and dried on air. Yield 82%. *Anal.* Calc. for $C_8H_{16}N_8CuPt$: C, 19.90; H, 3.34; N, 23.19. Found: C, 20.21; H, 3.79; N, 22.87%.

$[Cu(dmen)_2][Pt(CN)_4]$ (**2**). Similar to the synthesis of **1**, into stirring water–methanol solution (1:1) of $CuCl_2$

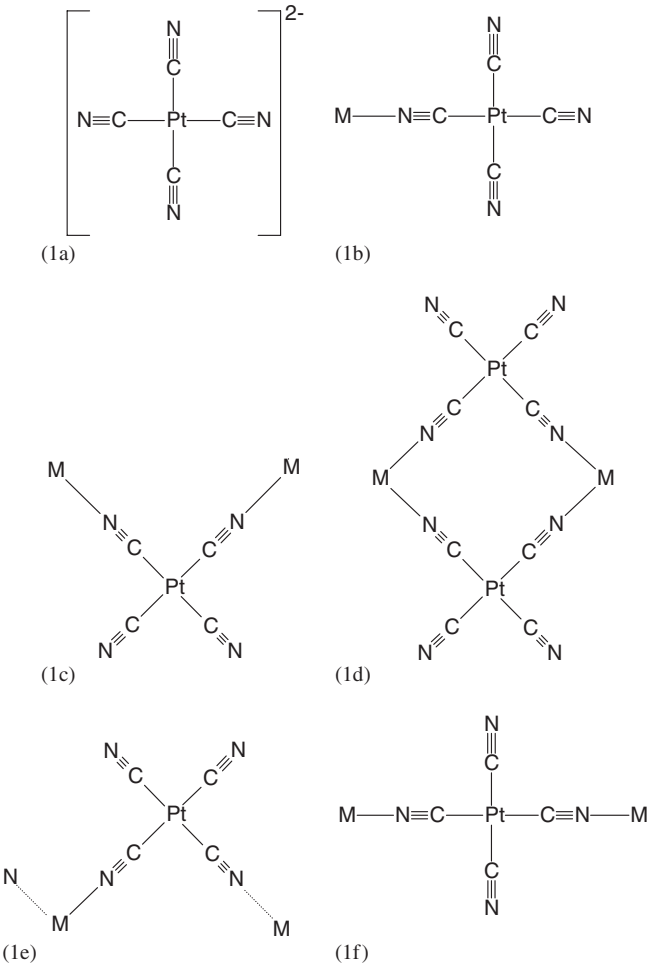


Scheme 1. Bonding modes of $[Pt(CN)_4]^{2-}$ anion. Dotted lines represent a propagation of the molecular or ionic structure to 1D (Scheme 1e and g) or 3D, structure (Scheme 1h, i and k).

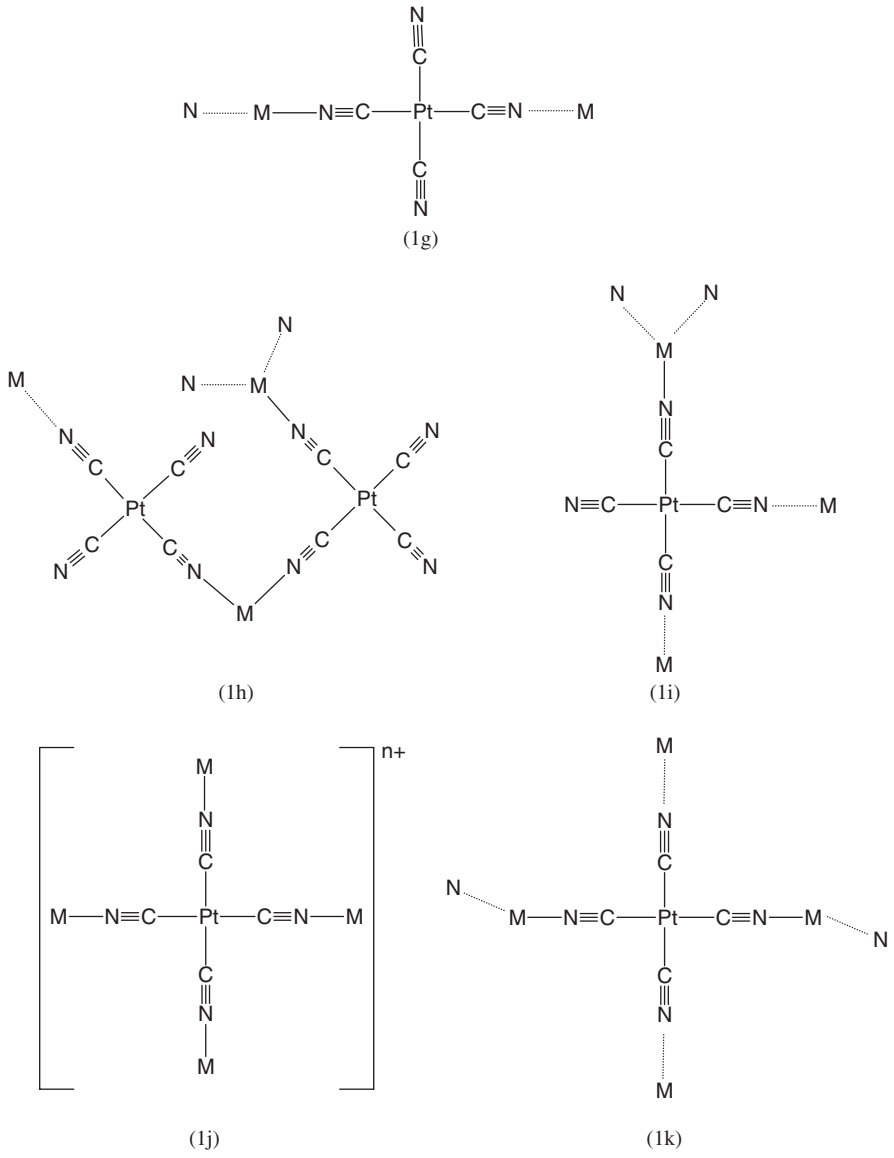


Scheme 1. (*Continued*)

(0.5 mmol), dmen (2 mmol) was added and finally after 30 min aqueous solution of $K_2[Pt(CN)_4]$ (0.5 mmol) was added. As a result a blue precipitate was immediately formed. This precipitate was dissolved by addition of 20 mL of concentrated ammonia solution to the reaction mixture. After 3 days, blue crystals of **2** were filtrated off and dried on air. Yield 93%. *Anal.* Calc. for $C_{12}H_{24}N_8CuPt$: C, 26.74; H, 4.49; N, 20.78. Found: C, 26.68; H, 5.05; N, 20.60%.

### 2.3. Physical measurements

Elemental analyses for C, H and N were carried out using an LECO CHNS-932. IR spectra were recorded on a MATTSON 5000 FTIR spectrometer by the method of KBr pellets in the range from 4000 to 400 $cm^{-1}$. Reflectance UV-VIS spectra were measured with Perkin Elmer UV/VIS/NIR Spectrometer Lambda 19. The thermal investigations were performed using NETZSCH STA 409C/CD thermal analyzer under air conditions with a heating rate of 10 °C/min to 900 °C. The electron spin resonance (ESR) experiment has been conducted at low temperatures in a home-built ESR spectrometer operating at 10 GHz. DPPH (2,2-diphenyl-1-picrylhydrazyl) was used as g-marker. Measurements of magnetic susceptibility and magnetization have been carried out on powdered samples using a commercial SQUID magnetometer in the temperature range from 2 to 300 K and in magnetic fields up to 7 T. The background contribution from the gelcap and core diamagnetic contribution to the magnetic moment of the sample have been subtracted. Specific heat of both materials was studied in the temperature range from 95 mK to 2.1 K in zero magnetic field using a dual-slope technique [21] in dilution refrigerator TLE 2000 made by

Oxford Instruments. $RuO_2$ resistor of Dale type with the nominal value of 1 kΩ calibrated against the commercial Lake Shore thermometer GR200A-30 was used for monitoring the temperature of the sample. The experimental inaccuracy of the specific heat measurements was less than 6%. The ESR and magnetic measurements have been carried out on powdered samples, while in thermodynamic experiments pelletized powder samples have been used. In addition, a small needle-like single crystal of complex **1** was used in the ESR investigations.

### 2.4. X-ray data collection and structure refinement

A summary of crystal data and structure refinement for **1** and **2** is presented in Table 1. The crystal structure of **1** was determined using an Oxford Diffraction diffractometer equipped with the CCD detector. Crysalis CCD [22] was used for data collection while Crysalis RED [22] was used for cell refinement, data reduction and absorption correction.

The crystal structure determination of **2** was carried out with Stoe Stadi-4 diffractometer. STADI4 [23] was used for data collection and cell refinement, X-RED [23] was used for data reduction. Both structures were solved by the direct method with SHELXS97 [24] and subsequent Fourier syntheses using SHELXL97 [24]. Anisotropic displacement parameters were refined for all non-H atoms. The H atoms were placed in calculated positions and refined riding on their parent C or N atoms with C–H distances of 0.97 for methylene and of 0.96 Å for methyl H atoms and of 0.90 Å for amino H atoms, and $U_{iso}(H) = 1.2U_{eq}$(C or N). A geometric analysis was performed using SHELXL97 and PARST [25]. DIAMOND [26] was used for molecular graphics.

## 3. Results and discussions

### 3.1. Infrared spectroscopy

The IR spectra of **1** and **2** comprise bands confirming the presence of all characteristic functional groups in the prepared complexes. In accordance with the substitution of two hydrogen atoms of one amino group in en (**1**) by two methyl groups in dmen (**2**), the IR spectrum of **1** contains more absorption bands originating from $\nu$(N–H) stretching vibrations and less absorption bands of stretching $\nu$(C–H) vibrations than the IR spectrum of **2**. Moreover, $\delta$, $\omega$ and $\sigma(CH_3)$ deformation vibrations are absent in **1**. Other bands confirming the presence of en and dmen in **1** and **2**, respectively, are listed in Table 2. Individual bands were assigned according to [27]. The presence of $[Pt(CN)_4]^{2-}$ anion in the prepared complexes is proved by $\nu$(C≡N) stretching vibrations whose positions are an important tool to distinguish between terminal and bridging character of cyano group. This band is observed at 2080 $cm^{-1}$ in ionic KCN [28]. Upon coordination to a metal the $\nu$(C≡N) shift to higher frequencies and the range of $\nu$(C≡N) for cyanoplatinates(II) with terminal cyano ligands extends from 2120 to 2140 $cm^{-1}$ [29]. Because cyano nitrogen lone pair resides in a mostly C≡N antibonding orbital, an increase of $\nu$(C≡N) in bridging cyanides is found and for bridged cyanoplatinates(II) it ranges from 2150 to 2210 $cm^{-1}$ [29]. According to this, the bands recorded at 2125 and 2130 $cm^{-1}$ in **1** and **2**, respectively, can be

Table 1
Crystal data and structure refinement of **1** and **2**

| | | |
|---|---|---|
| Empirical formula | $C_8H_{16}CuN_8Pt$ | $C_{12}H_{24}CuN_8Pt$ |
| Formula weight | 482.92 | 539.01 |
| Temperature | 120 K | 293(2) K |
| Wavelength | 0.71073 Å | 0.71073 Å |
| Crystal system | Triclinic | Monoclinic |
| Space group | $P\bar{1}$ | $P2_1/n$ |
| Unit cell dimensions | $a = 6.5254(3)$ Å, $\alpha = 106.919(5)^\circ$<br>$b = 7.2159(5)$ Å, $\beta = 91.223(4)^\circ$<br>$c = 8.1024(4)$ Å, $\gamma = 106.881(5)^\circ$ | $a = 6.7819(8)$ Å<br>$b = 13.8444(17)$ Å, $\beta = 97.618(11)^\circ$<br>$c = 9.2152(10)$ Å |
| Volume | 346.93(3) $Å^3$ | 857.59(17) $Å^3$ |
| $Z$ | 1 | 2 |
| Density (calculated) | 2.311 $g/cm^3$ | 2.087 $g/cm^3$ |
| Absorption coefficient | 11.598 $mm^{-1}$ | 9.396 $mm^{-1}$ |
| $F(000)$ | 227 | 518 |
| Crystal size | $0.27 \times 0.12 \times 0.06$ $mm^3$ | $0.35 \times 0.35 \times 0.19$ $mm^3$ |
| $\theta$ range for data collection | 3.28–27.49° | 2.67–24.99° |
| Index ranges | $-8 \leqslant h \leqslant 8$, $-9 \leqslant k \leqslant 9$, $-10 \leqslant l \leqslant 10$ | $-8 \leqslant h \leqslant 8$, $0 \leqslant k \leqslant 16$, $-10 \leqslant l \leqslant 10$ |
| Reflections collected | 6484 | 2995 |
| Independent reflections | 1564 [$R$(int) = 0.0197] | 1508 [$R$(int) = 0.0378] |
| Refinement method | Full-matrix least-squares on $F^2$ | Full-matrix least-squares on $F^2$ |
| Data/restraints/parameters | 1564/0/85 | 1508/0/104 |
| Goodness-of-fit on $F^2$ | 1.115 | 1.100 |
| Final $R$ indices [$I > 2\sigma(I)$] | $R_1 = 0.0120$, w$R_2 = 0.0275$ | $R_1 = 0.0265$, w$R_2 = 0.0743$ |
| $R$ indices (all data) | $R_1 = 0.0120$, w$R_2 = 0.0275$ | $R_1 = 0.0327$, w$R_2 = 0.0803$ |
| Largest diff. peak and hole | 0.634 and −0.922 e/$Å^3$ | 1.532 and −1.606 e/$Å^3$ |

Table 2
IR spectra of **1** and **2**

| | $[Cu(en)_2][Pt(CN)_4]$ (**1**) | $[Cu(dmen)_2][Pt(CN)_4]$ (**2**) |
|---|---|---|
| $\nu$(N–H) | 3335 vs | 3337 vs |
| | 3312 vs | 3273 vs |
| | 3281 vs | 3143 m |
| | 3254 sh | |
| | 3160 m | |
| $\nu$(C–H) | 2982 w | 3028 m |
| | 2961 m | 2973 m |
| | 2932 m | 2930 sh |
| | 2878 w | 2895 m |
| | | 2854 sh |
| | | 2816 m |
| $\nu$(C≡N) | 2125 vs | 2130 vs |
| | 2089 w, sh | 2088 w, sh |
| $\delta(NH_2)$ | 1597 s | 1584 s |
| $\delta(CH_2)$ | 1467 w | |
| | 1456 w | |
| $\delta(CH_3)$ | | 1462 s |
| $\omega(CH_2)$ | 1370 w | 1366 w |
| $\omega(NH_2)$ | 1324 m | 1323 w |
| $\tau(CH_2)$ | 1277 m | 1289 m |
| $\omega(CH_3)$ | | 1248 w |
| $\omega(NH_2)$ | 1165 m | 1190 m |
| $\tau(CH_3)$ | | 1134 vs |
| | | 1116 sh |
| $\tau(NH_2)$ | 1088 m | 1063 s |
| $\nu$(C–N) | 1033 vs | 1002 s |
| $\nu$(C–C) | 975 s | 940 s |
| $\sigma(CH_2)$ | 881 w | 894 m |
| $\sigma(NH_2)$ | 725 s | 783 s |
| $\sigma(CH_3)$ | | 654 s |
| $\delta$(chelate ring) | 536 m | 552 m |
| $\nu$(Pt–C) | 499 w | 502 m |
| | 473 w | 476 w |
| | 402 m | 401 s |

$\nu$—stretching, $\delta$—scissoring, $\omega$—wagging, $\tau$—twisting, $\sigma$—rocking vibrations, vs—very strong, s—strong, m—middle, w—weak vibrations, sh—shoulder.

assigned to $\nu$(C≡N) stretching vibrations of bridging cyano groups, while those at 2089 and 2088 $cm^{-1}$ in **1** and **2**, respectively, to terminal cyano groups. Surprisingly, although there are two bridging and two terminal cyano groups in the structures of **1** and **2**, the later bands are much weaker. On the other hand, in the case of $[Cu(en)_2][Ni(CN)_4]$ [17,30] and $[Cu(dmen)_2][Pd(CN)_4]$ [31] compounds only one $\nu$(C≡N) absorption band has been recorded. The same was observed in the spectra of $[Cu(L)_2][Ag_2(CN)_4]$ compounds where $L$ = en [32] or 1,2-diaminopropane [33] although both compounds contain both bridging and terminal cyano groups.

### 3.2. UV-VIS spectroscopy

The reflectance UV-VIS spectra of **1** and **2** (Fig. 1) were taken as described earlier. A broad asymmetric band with a maximum at 354 nm, observed in the spectrum of **1**, which could be assigned to $^2B_{1g} \rightarrow {}^2E_g$ transition is supportive of a

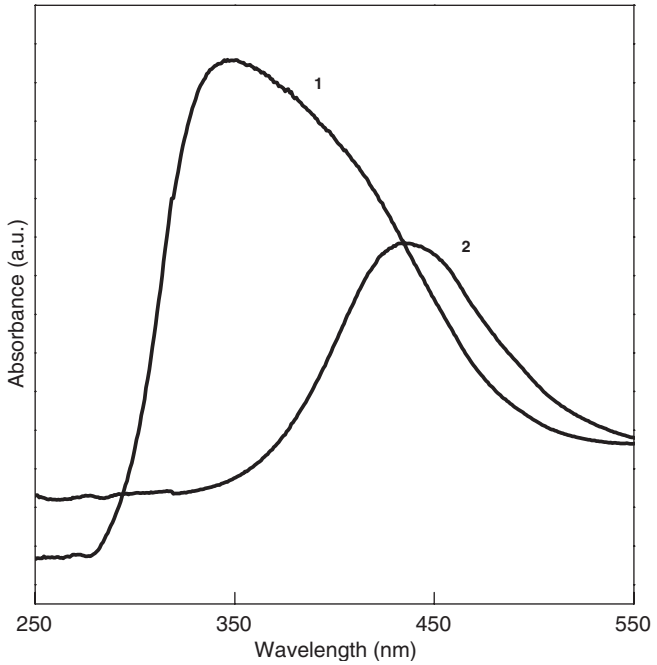


Fig. 1. UV-VIS spectra of **1** and **2**.

six-coordinated deformed octahedron with $CuN_6$ chromophoric group. The spectrum of **2** also consists of one broadband with the maximum at 435 nm and is assigned to $^2B_{1g} \rightarrow {}^2E_g$ transition in consistence with $CuN_6$ chromophore, likewise in **1**.

### 3.3. Thermal studies

Thermal decomposition of **1** and **2** is a multistage process. The thermal decomposition of **1** consists of two distinguished stages corresponding to the separated release of en molecules and cyano groups decomposing. Complex **1** is stable up to 246 °C. In the 246–417 °C temperature range, a weight loss of 25.3% corresponding to the release of two en molecules (calculated 24.9%) is observed during endothermic two-stage process (these stages are overlapped). The second step in the 417–448 °C temperature range, with observed weight loss of 21.2%, involves the decomposition of cyanides (calculated 21.6%). Their decomposition includes oxidation of four $CN^-$ groups to form two cyanogen molecules during reduction of one Pt(II) atom and one half of oxygen molecule from the air ambient. This process is accompanied by a strong exothermic effect as a consequence of the cyanogen molecules pyrolysis. The final thermal decomposition product is a mixture of CuO and metallic Pt (solid residue 56.8%; calculated 56.9%). The most probable thermal decomposition scheme for **1** is

$$[Cu(en)_2][Pt(CN)_4] \xrightarrow[-2en]{246-417\,^\circ C} CuPt(CN)_4$$

$$\xrightarrow[-2(CN)_2]{417-448\,^\circ C\,(O_2)} CuO + Pt.$$

The thermal decomposition of **2** is similar to the thermal decomposition of **1** and consists of two distinguished steps. In the first endothermic two-stage step a weight loss of 30.3% corresponding to the release of two dmen molecules (calculated 32.7%) is observed in the 193–427 °C temperature range. The decomposition proceeds continuously into the second strongly exothermic step which is finished at 461 °C with observed weight loss of 22.3% which corresponds to the decomposition of cyanides (calculated 19.3%). Their decomposition includes the oxidation of four $CN^-$ groups to form two cyanogen molecules during the reduction of one Pt(II) atom and one half of oxygen molecule from the air ambient. The final thermal decomposition product is a mixture of CuO and metallic Pt (solid residue 51.5%; calculated 51.0%). The most probable thermal decomposition scheme for **2** is

$$[Cu(dmen)_2][Pt(CN)_4] \xrightarrow[-2dmen]{193-427\,^\circ C} CuPt(CN)_4$$

$$\xrightarrow[-2(CN)_2]{427-461\,^\circ C\,(O_2)} CuO + Pt.$$

### 3.4. X-ray crystallography

X-ray analysis has revealed that the crystal structure of **1** consists of 1D zigzag chains running in [111] direction. An ORTEP view of the complex **1** is depicted in Fig. 2 with the atomic numbering scheme. In the structure, both Cu(II) and Pt(II) ions occupy sites of inversion centers. The Cu(II) ion is six-coordinate, complexed with the four nitrogen atoms of en ligands in the equatorial plane and the two nitrogen atoms from bridging cyano groups in the axial positions, respectively. The Cu–N bond distances in the equatorial plane have an average value of 2.022(7) Å (Table 3), while weak axial interactions, a characteristic of $d^9$ systems, give rise to a Cu–N bond length of 2.537(2) Å. The Cu–N bonds in the axial positions are slightly tilted from the normal to the $CuN_4$ plane (2.74°), forming a slightly distorted and tetragonally elongated octahedral geometry. Because of the inversion center, all N–Cu–N bond angles formed by two face to face nitrogen atoms, no matter whether they are located in the equatorial plane or in the axial positions, are 180.0°. By contrast, the Pt(II) ion possesses a square planar coordination surrounding in which it is coordinated to the four carbon atoms from four cyano groups. Despite the division of Pt–C bonds into two pairs, depending on CN groups (bridging or terminal) their bond lengths are similar with the average value of 1.997(4) Å. Alike the Cu(II) atom, the C–Pt–C bond angles are of 180.0° due to the presence of the inversion center. Two of the four cyano groups from a tetracyanoplatinate(II) ion are connected to two different Cu(II) moieties in a trans mode that leads to a zigzag chain with the bond angle of 120.6(2)° for the Cu–N2–C2. The interchain HBs N3–H3B···$N2^i$ and N4–H4B···$N1^{ii}$ with length of 3.220(3) and 3.126(3) Å, respectively (Table 4), connect the neighboring chains resulting in a 3D network. Moreover, the N4–H4A···N1 distance of 3.250(3) Å indicates the HB interaction within the chain. The HB system in **1** is shown in Fig. 3. If we compare the HB system in **1** with the HB system observed in the reference $[Cu(en)_2][Ni(CN)_4]$ compound [17] we can see that the HB system in **1** was not reduced because both the intrachain HB and the interchain HB between N3 and $N2^i$ atoms connecting the chains into sheets are present in the reference compound, too. Moreover, interchain HB between N4 and $N1^{ii}$ atoms connecting the sheets in the 3D network in **1** was not observed in the reference compound at all.

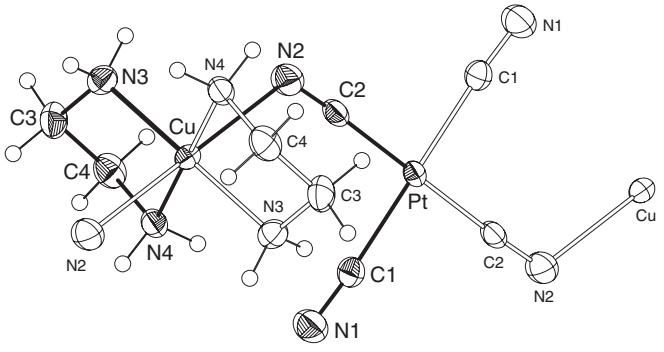


Fig. 2. The crystal structure of **1** with displacement ellipsoids (75% probability) and atom labeling.

Table 3
Selected bond lengths (Å) and bond angles (deg) of **1**

| | |
|---|---|
| Pt–C2 | 1.994(2) |
| Pt–C1 | 2.000(2) |
| C2–N2 | 1.153(3) |
| N1–C1 | 1.154(3) |
| N2–Cu | 2.5379(19) |
| Cu–N4 | 2.0170(19) |
| Cu–N3 | 2.0274(17) |
| C2–Pt–C1 | 87.75(8) |
| N2–C2–Pt | 177.1(2) |
| N1–C1–Pt | 176.01(19) |
| C2–N2–Cu | 120.64(15) |
| N4–Cu–N3 | 84.39(7) |
| N4–Cu–N2 | 91.44(7) |
| N3–Cu–N2 | 87.80(7) |

Table 4
Hydrogen bonds of **1** (Å and deg)

| D–H···A | D–H | H···A | D···A | D–H···A |
|---|---|---|---|---|
| N4–H4A···N1 | 0.90 | 2.38 | 3.250(3) | 161.6 |
| N3–H3B···$N2^i$ | 0.90 | 2.42 | 3.220(3) | 147.6 |
| N4–H4B···$N1^{ii}$ | 0.90 | 2.31 | 3.126(3) | 151.2 |

Symmetry transformations used to generate equivalent atoms: i: $-x$, $-y+1$, $-z$, ii: $-x+1$, $-y$, $-z$.

Complex **2** exhibits an analogous solid-state structure as complex **1**, see Fig. 4. The Cu(II) ion also exhibits a slightly

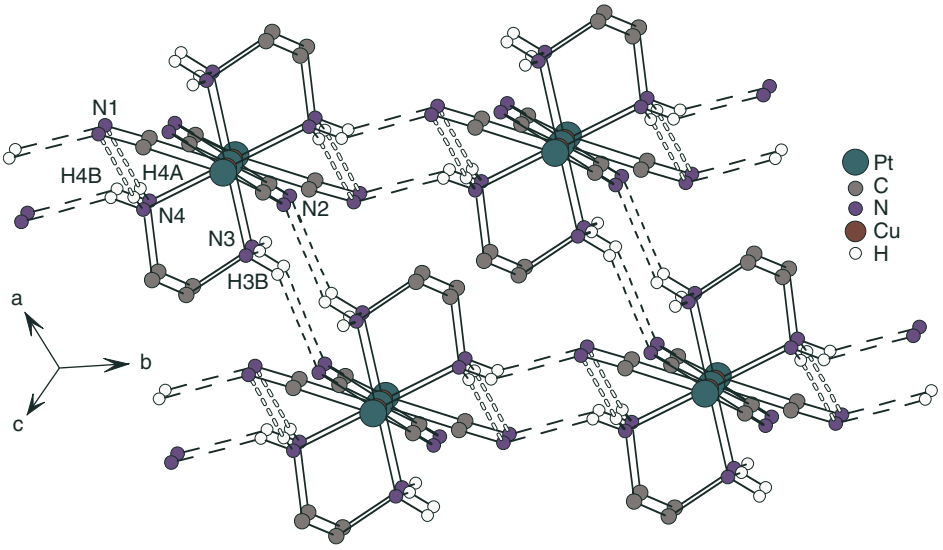


Fig. 3. HB system in **1** viewed along the chain direction. The HBs connecting chains into sheets are represented by black short dashed lines, the HBs connecting sheets into 3D structure are represented by black long dashed lines while intrachain HBs are represented by empty dashed lines. Only hydrogen atoms of amino groups are shown because of clarity.

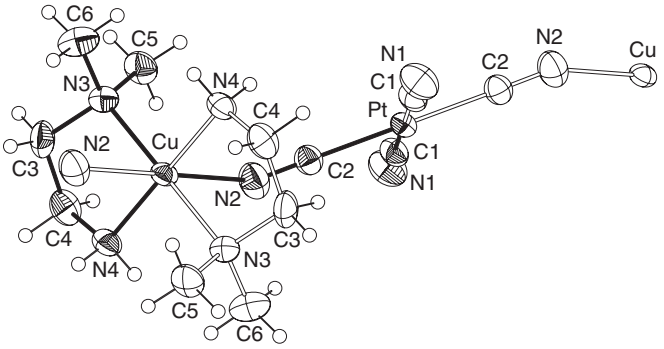


Fig. 4. The crystal structure of **2** with displacement ellipsoids (45% probability) and atom labeling.

distorted (the tilting angle between the apical axis and the normal to the $CuN_4$ plane is 3.46°) and tetragonally elongated octahedral coordination geometry. In contrast to **1**, the Cu–N bond distances in the equatorial plane are not of the same length as the Cu–N3 bond of 2.115(4) Å is significantly longer than the Cu–N4 bond of 1.984(4) Å. This difference is caused by the steric repulsion of two methyl groups bonded to nitrogen N3 atom. The Cu–N bond distances in the axial positions are 2.600(5) Å due to Jahn–Teller effect. The bond distances and angles for **2** are given in Table 5. Pt(II) ion has the same coordination environment as in **1** with the average Pt–C bond lengths of 1.993(5) Å. The basic features of the molecular structure of **2** are the same as that of **1** consisting of zigzag chains running in [101] direction with the Cu–N2–C2 bond angle of 137.5(5)°. Similar to **1**, the interchain HB N4–H4A···N1 with length of 3.351(6) Å (Table 6), connects the chains into 2D sheets (Fig. 5). However, the formation of intrachain HB is suppressed due to the presence of two methyl groups bonded on nitrogen N3 atom. The same

Table 5
Selected bond lengths (Å) and bond angles (deg) of **2**

| | |
|---|---|
| Cu–N4 | 1.984(4) |
| Cu–N3 | 2.115(4) |
| Cu–N2 | 2.600(5) |
| Pt–C2 | 1.989(6) |
| Pt–C1 | 1.996(5) |
| C2–N2 | 1.146(8) |
| C1–N1 | 1.147(6) |
| N4–Cu–N3 | 85.00(16) |
| N4–Cu–N2 | 88.55(17) |
| N3–Cu–N2 | 93.00(15) |
| C2–Pt–C1 | 90.0(2) |
| N2–C2–Pt | 179.3(5) |
| N1–C1–Pt | 179.0(4) |
| C2–N2–Cu | 137.5(5) |

Table 6
Hydrogen bonds of **2** (Å and deg)

| D–H···A | D–H | H···A | D···A | D–H···A |
|---|---|---|---|---|
| N4–H4A···N1$^{i}$ | 0.90 | 2.61 | 3.351(6) | 140.0 |

Symmetry transformation used to generate equivalent atoms: i: $-x+2$, $-y+1$, $-z+1$.

type of the HB system was observed also in the reference $[Cu(dmen)_2][Ni(CN)_4]$ compound [19].

### 3.5. Magnetic properties

The ESR spectra obtained at 4.2 K on powdered samples have been analyzed within a simple model including dipolar interactions, magnetic field and isotropic exchange coupling [34]. The best fit to the experimental data using

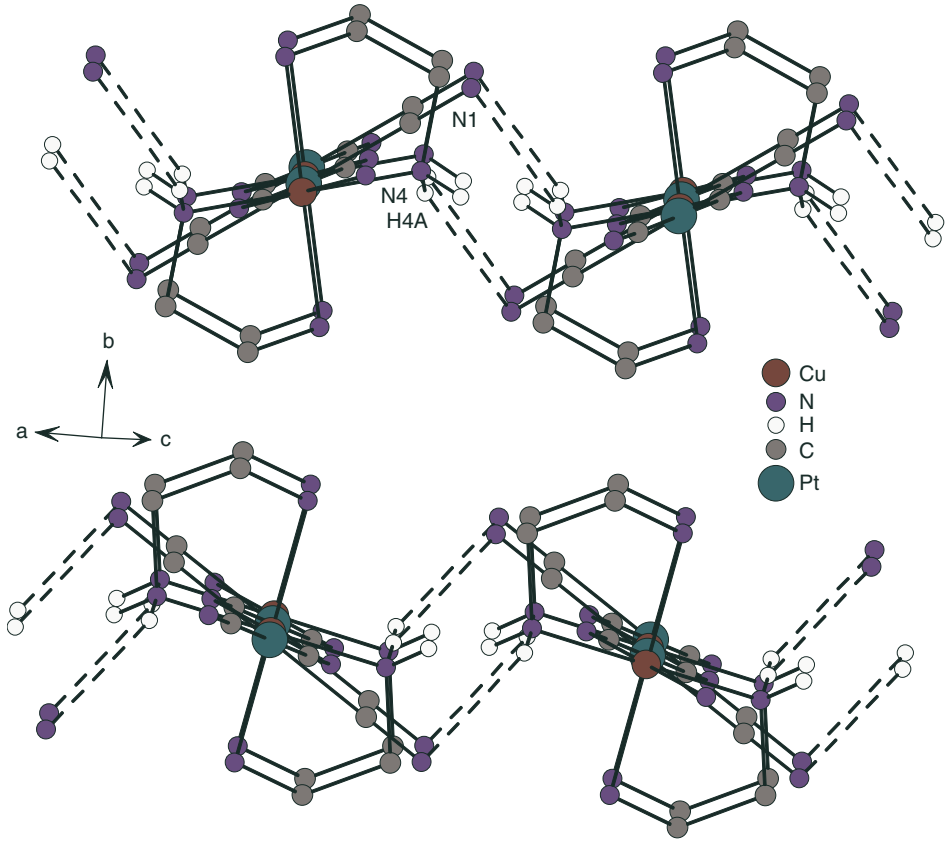


Fig. 5. HB system in **2** viewed along the chain direction. The HBs connecting chains into sheets are represented by black short dashed lines. Methyl groups are omitted and only hydrogen atoms of N4 amino group are shown because of clarity.

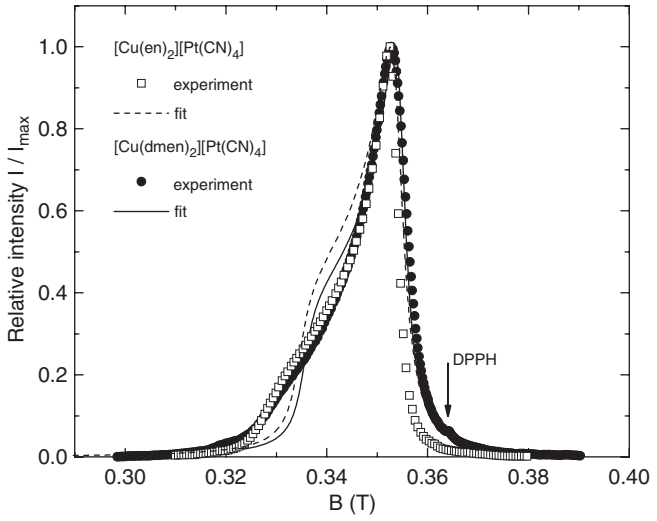


Fig. 6. Comparison of the experimental ESR spectra of complex **1** (squares) and complex **2** (circles) with the simple theoretical prediction [34] (dashed line for complex **1**, while solid line is for complex **2**). The values of resonance fields and halfwidths obtained from the fits are in Table 7.

least-squares method (Fig. 6) has been obtained for the values of resonance fields and the halfwidth of the resonance line, $\Delta B$ presented in Table 7. Slightly anisotropic $g$-factor values corresponding to the resonance fields (also in Table 7) are consistent with the axial distortion of the coordination octahedron and are typical for spin 1/2 Cu(II) ions. The deviations between the fit and data might be attributed to the low-dimensional character of the magnetic subsystem and/or orthorhombic anisotropy of the $g$-factor resulting from a deformation of the local octahedron.

The angular dependence of $g$-factor of the complex **1** shown in Fig. 7 has been obtained from resonance fields of ESR spectra measured on a single crystal. Magnetic field was oriented within the $a'c'$ plane. The $c'$ direction is the longest edge of the crystal, while $a'$ is a shortest edge approximately perpendicular to the $c'$ direction. The experimental data have been fitted to the formula

$$g^2 = g_{||}^2 \cos^2(\theta - \theta_0) + g_{\perp}^2 \sin^2(\theta - \theta_0), \quad (1)$$

where $\theta$ is an angle between the magnetic field and the local $z$-axis and $\theta_0$ is the angle between the $c'$ direction and local $z$-axis (Fig. 7). The best agreement was achieved for the values of $\theta_0 = 23^\circ$, $g_{||} = 2.24 \pm 0.01$ and $g_{\perp} = 2.07 \pm 0.01$ close to the ones obtained from the analysis of powder spectra. Additional X-ray experiments were performed to find a proper orientation of the single crystal. Analysis of the X-ray data provided the estimation of the angle between the local $z$-axis and $c'$ direction, being equal to about 20°. This value is in good agreement with the angle

Table 7
Resonance fields and $g$-factor values obtained from powder ESR spectra

| | $B_{\|\|}$ (T) | $B_{\perp}$ (T) | $\Delta B$ (mT) | $g_{\|\|}$ | $g_{\perp}$ |
|---|---|---|---|---|---|
| $[Cu(en)_2][Pt(CN)_4]$ | 0.3346±0.001 | 0.3535±0.001 | 2.0±0.2 | 2.21±0.01 | 2.10±0.01 |
| $[Cu(dmen)_2][Pt(CN)_4]$ | 0.3350±0.001 | 0.3545±0.001 | 1.9±0.2 | 2.20±0.01 | 2.08±0.01 |

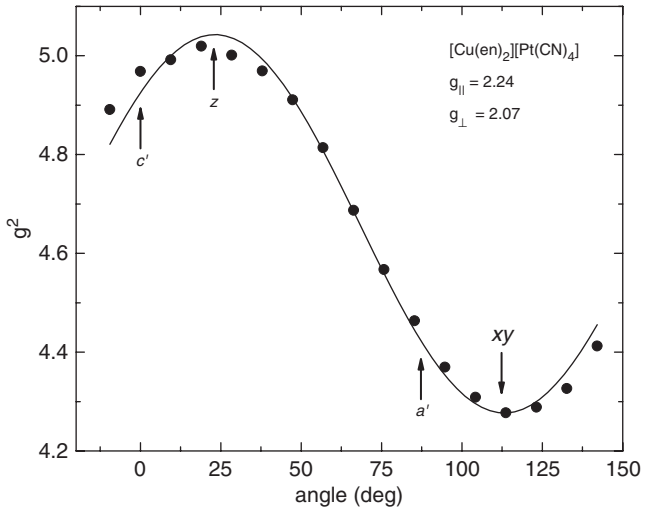


Fig. 7. Angular dependence of $g^2$-factor value obtained from the ESR spectra of single crystal of the complex **1** (full circles). The solid line represents the least-squares fit to Eq. (1).

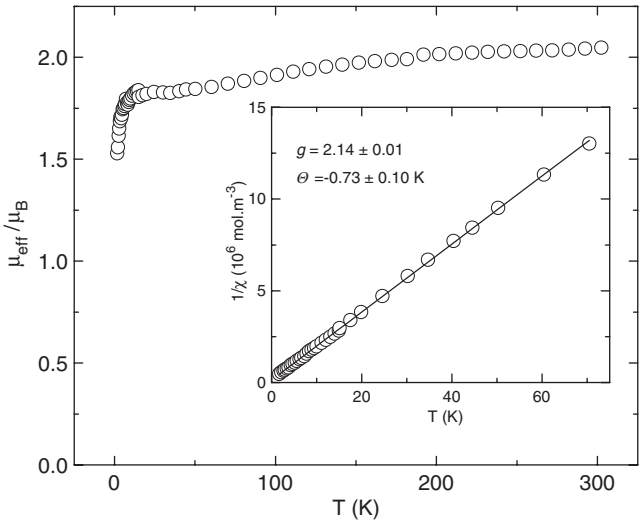


Fig. 8. Effective magnetic moment of complex **2**. Inset shows the temperature dependence of inverse susceptibility (circles) with a fit to the Curie–Weiss law (solid line).

23° found from the fitting procedure using Eq. (1) and corresponds to the position of the maximum $g$-factor value found in the $a'c'$ plane. Consequently, the position of a minimum $g$-factor value in the same plane might be ascribed to the orientation within the equatorial $xy$-plane of the local octahedron. The results confirm that the electronic ground state of Cu(II) ion is described by a wave function of $d_{z^2}$ symmetry and the exchange paths will propagate along the directions determined by the lobes of the $d_{x^2-y^2}$ orbital.

Magnetic susceptibilities of powdered samples of both materials measured at 0.1 T were corrected for the diamagnetic contribution of the materials which was estimated, using Pascal's constants, to be $\chi_{DIA} = -2.9586 \times 10^{-9}\,m^3/mol$ for complex **1**, while $\chi_{DIA} = -2.396 \times 10^{-9}\,m^3/mol$ for complex **2**. From susceptibility at $T = 300$ K, the effective magnetic moment may be quantified and yields values that are typical for a Cu(II) cation with $d^9$ configuration, namely $\mu_{eff}/\mu_B = 1.95$ for complex **1** [35] and $\mu_{eff}/\mu_B = 1.99$ for complex **2** (Fig. 8). No difference between the susceptibility of zero-field cooled (ZFC) and field-cooled sample has been observed down to 2 K for both materials, which suggests that no long-range order appears above 2 K. The temperature dependence of the susceptibility is characterized by Curie-like behavior without the short-range order maximum expected at low temperatures for the low-dimensional system with antiferromagnetic exchange coupling. Consequently, only an estimate of the effective strength of the exchange coupling $zJ/k_B$, where $z$ is the number of the nearest neighbors, by fitting the Curie–Weiss law to the experimental data in the temperature range 2–75 K is obtained. The fit yields the values $zJ/k_B = -1.6$ K and $g = 2.15$ for complex **1** [35], while $zJ/k_B = -2.92$ K and $g = 2.14$ for complex **2** (inset in Fig. 8).

In the work [35], it has been shown that the field dependence of the magnetization of the complex **1** is close to the saturation at 7 T and indicates a free spin behavior at 2 K, while the magnetization of complex **2** measured at 4.75 K shows no saturation up to 6 T (Fig. 9). The comparison of the experimental data with the free spin model suggests the presence of weak antiferromagnetic exchange coupling. The results of magnetization measurements are consistent with the estimation of the effective exchange coupling from the inverse susceptibility, where the magnitude of effective exchange coupling in complex **2** is higher than in complex **1**.

The specific heat of both materials has been investigated in zero magnetic field in the temperature range 95 mK–2.0 K and 95 mK–0.80 K, for complex **1** and complex **2**, respectively, with the aim to resolve the magnetic structure and dimensionality of the systems. The temperature dependence of the magnetic specific heat of complex **1** displays a round maximum at $T_{max} = 0.28$ K and $\lambda$-like anomaly, associated with long-range ordering, at $T_\lambda = 0.18$ K, while the complex **2** shows only an indication

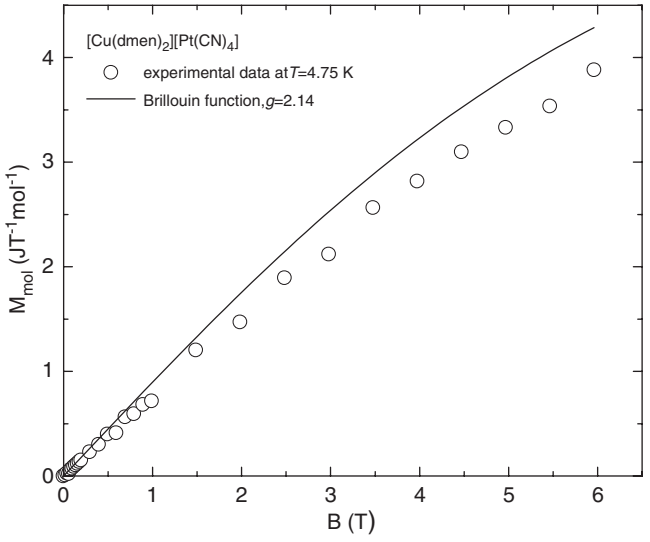


Fig. 9. Field dependence of the magnetization of complex **2** measured at 4.75 K (circles) compared to the Brillouin function for $g = 2.14$ obtained from Curie–Weiss fit of the inverse susceptibility (solid line).

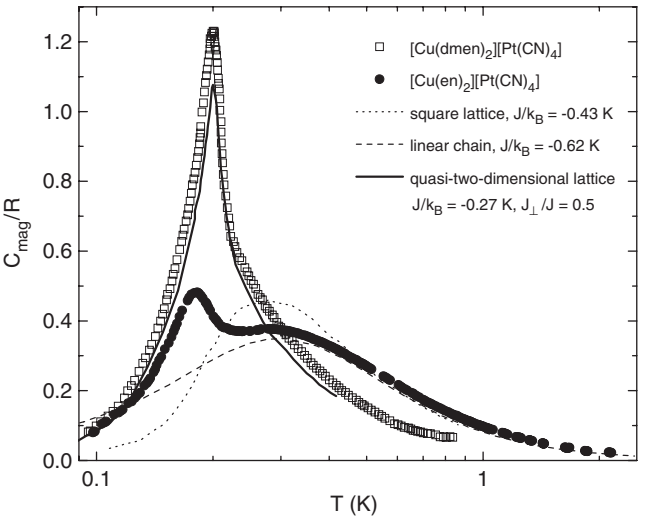


Fig. 10. Magnetic specific heat of complex **1** compared to the HAF square lattice model with $J/k_B = -0.43$ K (dotted line), while dashed line represents the HAF linear chain model with $J/k_B = -0.62$ K. The solid line represents quasi-two-dimensional square lattice HAF model with intralayer $J/k_B = -0.27$ K and interlayer $J_\perp/J = 0.5$ describing the behavior of magnetic specific heat of the complex **2**.

of the round maximum overlapped with a dominating $\lambda$-like anomaly at $T_\lambda = 0.2$ K (Fig. 10). The lattice contribution to the total specific heat of both materials was subtracted after fitting high temperature region to the equation $C = aT^{-2} + bT^3$, where $aT^{-2}$ describes the high-temperature expansion of magnetic specific heat, while $bT^3$ represents the low-temperature description of the lattice contribution in the Debye approximation. After subtraction of the lattice contribution, the magnetic entropy $S_m$ has been calculated from the experimental data with simple approximations used for $T \to 0$ and $T \to \infty$. The calculated

Table 8
Magnetic entropy of studied materials calculated from experimental specific heat

| | $S_m$ (J/K/mol) | $S_m/S_{theor}$ | Entropy removed above $T_\lambda$ |
|---|---|---|---|
| $[Cu(en)_2][Pt(CN)_4]$ | 5.75 | 0.91 | 4.61 (80%) |
| $[Cu(dmen)_2][Pt(CN)_4]$ | 6.1 | 1.06 | 3.64 (60%) |

values of the magnetic entropy, $S_m$, with respect to the theoretically predicted value $S_{theor} = R\ln(2S+1) = 5.76$ J/K/mol for magnetic system with spin $S = 1/2$ are shown in Table 8. The magnetic entropy removed above $T_\lambda$ in both materials represents more than 50% of the total magnetic entropy suggesting low-dimensional character of the studied systems. However, the magnetic dimensionality of the complex **2** with 60% of total entropy removed above $T_\lambda$ is more likely close to the 3D magnetic system.

Considering the topology of covalent and possible HBs the magnetic specific heat of the complex **1** has been compared to the theoretical models for Heisenberg antiferromagnetic (HAF) linear chain [36] and isotropic HAF square lattice [37,38] (Fig. 10). The values of exchange coupling parameters obtained from the comparison were $J/k_B = -0.62$ and $-0.43$ K for HAF linear chain model and HAF square lattice model, respectively. These values are in agreement with the estimation of the effective strength of the exchange coupling from the Curie constant. The height of the maximum at $T_{max} = 0.28$ K suggests that the system might be described by the 2D model of the spatially anisotropic square lattice [39], where linear chains are coupled by the interchain exchange coupling $J'$. This model coincides well with the geometry of the HBs net in the structure of complex **1**, i.e. intrachain interaction $J$ might be mediated by doubled Cu–N4–H4A$\cdots$N1$\cdots$H4B–N4–Cu exchange path, while $J'$ runs along Cu–N3–H3B$\cdots$N2–Cu pathway. However, the theoretical prediction for the temperature dependence of the magnetic specific heat of the aforementioned model is not available yet, thus, we are unable to estimate the interchain coupling $J'$ in complex **1** from the measured data set.

The magnetic specific heat of the complex **2** can be described by the theoretical model for quasi-two-dimensional HAF square lattice [40] with in-plane coupling $J$ and varying interplane coupling $J_\perp < J$. From the comparison of the experimental data to the theoretical model we have obtained the values $J/k_B = -0.27$ K and $J_\perp/J = 0.5$ (Fig. 10) suggesting strong influence of interplane coupling in complex **2**, driving the system into transition to the three-dimensional long range order. This result is supported by the 60% ratio of the magnetic entropy removed above the $T_\lambda$. The strength of exchange coupling is also in agreement with the estimation of effective exchange coupling from the Curie–Weiss fit of the susceptibility. The difference between the experimental data and

theoretical prediction can be ascribed to the presence of slightly stronger interlayer coupling $J_\perp$ in complex **2** than that taken into account in the available theoretical prediction and finite size calculations [40].

## 4. Conclusions

The X-ray analysis of violet crystals of $[Cu(en)_2][Pt(CN)_4]$ (**1**) and blue crystals of $[Cu(dmen)_2][Pt(CN)_4]$ (**2**) revealed that both structures are formed by infinite zigzag chains. The covalent chains are built of Cu(II) atoms linked by $[Pt(CN)_4]^{2-}$ anions in the [111] and [101] direction, respectively. The Cu(II) atoms are hexacoordinated by four nitrogen atoms in the equatorial plane from two molecules of bidentate ligands $L$ with average Cu–N distance of 2.022(2) and 2.049(4), respectively. Axial positions are occupied by two nitrogen atoms from bridging $[Pt(CN)_4]^{2-}$ anions at longer Cu–N distance of 2.537(2) and 2.600(5) Å, respectively.

The chains are bound into sheets in both complexes by relatively strong HBs of N–H⋯N type. Moreover, another N–H⋯N HB is found between these sheets in **1** and thus 3D structure is finally formed. Contrary to the 3D character of this structure the specific heat analysis suggests that the magnetic structure in this complex can be approximated by the spatially anisotropic square lattice Heisenberg model with $J/k_B \approx -0.5$ K similar as in the compound $[Cu(en)_2][Ni(CN)_4]$ [17]. However, the interchain coupling $J'$ is weaker in complex **1**. The 2D magnetic structure can be explained by the fact that the magnetic $d_{x^2-y^2}$ orbital is oriented within the equatorial plane of the local octahedron due to the Jahn–Teller distortion and is not involved in the covalent bonds. Consequently, the exchange path between Cu(II) atoms is preferred through HBs between the chains and not through the covalent bonds within the chain.

The structure of **2** remains 2D as the second N–H⋯N bond binding the neighboring sheets is missing. On the other hand, the replacement of two hydrogen atoms by methyl groups on N2 atom in en ligands supports the creation of a dense network of weak C–H⋯N HBs increasing the magnetic dimensionality. Consequently, the 2D magnetic behavior is strongly overlapped by interlayer effects due to the weak HBs network.

Finally we can conclude that although the use of bulky $[Pt(CN)_4]^{2-}$ anion instead of $[Ni(CN)_4]^{2-}$ anion resulted in a different HBs system, HBs were not suppressed at all. Therefore, we intend to use in our next work other ligands $L$ which are definitely unable to form strong hydrogen bridges, like 1,10-phenanthroline, 2,2′-bipyridine or $N,N,N',N'$-tetramethylethylenediamine.

## Acknowledgments

This work was supported by the grants of the Slovak Grant Agency VEGA Nos. 1/2470/05 and 1/3027/06, by Research and Development Support Agency APVV No. 20-005204 and by the Grant Agency of the Czech Republic, Grant 202/05/0421. One of the authors (M.V.) thanks Socrates/Erasmus stipend program for financial support and hospitality of Martin-Luther-University and E.Č. thanks DAAD for financial support and hospitality of University of Bayreuth during the magnetic measurements. The financial support of US Steel—DZ Energetika Košice is acknowledged.

## Supplementary material

CCDC 299194 & 299195 contains the supplementary crystallographic data for this paper. These data can be obtained free of charge via http://www.ccdc.cam.ac.uk/conts/retrieving.htmL (or from the CCDC, 12 Union Road, Cambridge CB2 1EZ, UK; fax: +44 1223 336033; e-mail: deposit@ccdc.cam.ac.uk).

## References

[1] J. McCleverty, T. Meyer (Eds.), Comprehensive Coordination Chemistry II, vol. 1, Elsevier, Amsterdam, 2004.
[2] P. Vitoria, J.I. Beitia, J.M. Gutierrez-Zorrilla, E.R. Saiz, A. Luque, M. Insausti, J.J. Blanco, Inorg. Chem. 41 (2002) 4396.
[3] J.A. Brozik, B.L. Scott, B.I. Swanson, Inorg. Chim. Acta 294 (1999) 275.
[4] M.-L. Flay, H. Vahrenkamp, Eur. J. Inorg. Chem. (2003) 1719.
[5] I. Muga, J.M. Gutierrez-Zorrilla, P. Vitoria, P. Roman, F. Lloret, Polyhedron 21 (2002) 2631.
[6] L.R. Falvello, M. Tomas, Chem. Commun. (1999) 273.
[7] M.M. Olmstead, M.A. Lee, J.R. Stork, Acta Crystallogr. E 61 (2005) m1048.
[8] G.N. Richardson, U. Brand, H. Vahrenkamp, Inorg. Chem. 38 (1999) 3070.
[9] M. Munakata, J.C. Zhong, I. Ino, T. Kuroda-Sowa, M. Maekawa, Y. Suenaga, N. Oiji, Inorg. Chim. Acta 317 (2001) 268.
[10] D.W. Knoeppel, S.G. Shore, Inorg. Chem. 35 (1996) 1747.
[11] D.W. Knoeppel, S.G. Shore, Inorg. Chem. 35 (1996) 5328.
[12] M.-L. Flay, H. Vahrenkamp, Z. Anorg. Allg. Chem. 630 (2004) 2508.
[13] R.W. Gable, B.F. Hoskins, R. Robson, Chem. Commun. (1990) 762.
[14] J.P. Zhang, R.S. Wang, M. Baumgarten, Mol. Cryst. Liq. Cryst. 306 (1997) 119.
[15] R. Boča, Coord. Chem. Rev. 173 (1998) 167.
[16] J. Lokaj, K. Györyová, A. Sopková, J. Sivý, V. Kettmann, V. Vrábel, Acta Crystallogr. C 47 (1991) 2447.
[17] M. Orendáč, A. Orendáčová, J. Černák, A. Feher, Solid State Commun. 94 (1995) 833.
[18] J. Černák, J. Skoršepa, K.A. Abboud, M.W. Meisel, M. Orendáč, A. Orendáčová, A. Feher, Inorg. Chim. Acta 326 (2001) 3.
[19] J. Kuchár, J. Černák, Z. Mayerová, P. Kubáček, Z. Žák, Solid State Phenom. 90 (2003) 323.
[20] G.B. Kaufmann, Inorg. Synth. 9 (1967) 182.
[21] S. Riegel, G. Webber, J. Phys. E 19 (1986) 790.
[22] Oxford Diffraction, Crysalis CCD and Crysalis RED, Oxford Diffraction Ltd., Oxford, UK, 2004.
[23] Stoe & Cie, STADI4 (Version 1.06) and X-RED (Version 1.07), Stoe & Cie, Darmstadt, Germany, 1996.
[24] G.M. Sheldrick, SHELXS97 and SHELXL97, University of Göttingen, Göttingen, Germany, 1997.
[25] M. Nardelli, J. Appl. Crystallogr. 28 (1995) 659.
[26] K. Brandenburg, DIAMOND (Release 2.1e) Crystal Impact GbR, Bonn, Germany, 2000.
[27] Z. Gabelica, Spectrochim. Acta 32A (2) (1976) 337.
[28] K. Nakamoto, Infrared and Raman Spectra of Inorganic and Coordination Compounds, Part B: Applications in Coordination,

Organometallic, and Bioinorganic Chemistry, fifth ed., Wiley, New York, 1997, p. 105.
[29] A.M. Golub, H. Köhler, V.V. Skopenko, Chemistry of Pseudohalides, Elsevier, Amsterdam, 1986.
[30] K. Seits, S. Peschel, D. Babel, Z. Anorg. Allg. Chem. 627 (2001) 929.
[31] J. Kuchár, J. Černák, K.A. Abboud, Acta Crystallogr. C 60 (2004) m492.
[32] J. Černák, J. Chomič, P. Gravereau, A. Orendáčová, M. Orendáč, J. Kováč, A. Feher, C. Kappenstein, Inorg. Chim. Acta 281 (1998) 134.
[33] L'. Triščíková, I. Potočňák, J. Chomič, P. Baran, Trans. Met. Chem. (2006), accepted for publication.
[34] J.A. Ibers, J.D. Swalen, Phys. Rev. 127 (1962) 1914.
[35] K. Tibenská, A. Orendáčová, E. Čižmár, J.-H. Park, Š. Lančarič, M. Orendáč, A.G. Anders, M. Vavra, I. Potočňák, A. Feher, M.W. Meisel, Phys. Stat. Sol. B 243 (2006) 281.
[36] L.J. de Jongh, A.R. Miedema, Adv. Phys. 23 (1974) 1.
[37] M.S. Makivic, H.-Q. Ding, Phys. Rev. B 43 (1991) 3562.
[38] B. Bernu, G. Misguich, Phys. Rev. B 63 (2001) 134409.
[39] Y.J. Kim, R.J. Birgenau, Phys. Rev. B 62 (2000) 6378.
[40] P. Sengupta, A.W. Sandvik, R.R.P. Singh, Phys. Rev. B 68 (2003) 094423.